Proceedings of the Combustion Institute, Volume 28, 2000/pp. 1793–1800

MORPHOLOGY AND BURNING RATES OF EXPANDING SPHERICAL FLAMES IN H_2/O_2/INERT MIXTURES UP TO 60 ATMOSPHERES

S. D. TSE, D. L. ZHU AND C. K. LAW

Department of Mechanical and Aerospace Engineering Princeton University
Princeton, NJ 08544, USA

Recognizing that previous experimental studies on constant-pressure, outwardly propagating, spherical flames with imaging capability were limited to pressures less than about 5 atm, and that pressures within internal combustion engines are substantially higher, a novel experimental apparatus was designed to extend the environmental pressure to 60 atm. Results substantiate previous observations of the propensity of cell formation over the flame surface due to hydrodynamic and diffusive-thermal instabilities and provide convincing evidence that wrinkled flame is the preferred mode of propagation in hydrogen/air mixtures in environments with pressures above only a few atmospheres. It is further shown that, by using helium as the diluent, and by reducing the oxygen concentration of the combustible, diffusional-thermal instability can be mostly suppressed and the hydrodynamic instability delayed. Stretch-free laminar flame speeds were subsequently determined for such smooth flames up to 20 atm and were compared with the calculated values, allowing for detailed chemistry and transport.

Introduction

The laminar flame speed, s_u^0, is perhaps one of the most fundamentally and practically important thermochemical parameters of a combustible mixture. Practically, it indicates the rate with which the combustible mixture is consumed by a propagating laminar flame and is frequently needed in the assessment of various flame phenomena such as ignition, quenching, stabilization, and turbulent flame propagation. Fundamentally, it embodies the basic diffusive and reactive information about the combustible and as such has recently been used extensively as an important parameter in the partial validation of reaction mechanisms. The last point is of particular significance because it indicates the potential of using any mixture to extract the fundamental chemical information, not necessarily ones involving air as the oxidizer or nitrogen as the inert.

While extensive efforts have been expended toward the determination of s_u^0 over the years, accurate, stretch-free data have only recently become available since Wu and Law [1] first identified the importance of stretch and proposed the methodology to systematically subtract it out from measured values. However, due to the various limitations to be discussed later, stretch-free data have only been determined for pressures up to a few atmospheres. Since combustion processes within internal combustion engines take place in environments of highly elevated pressure substantially above atmospheric pressure, there is clearly the need for high-pressure s_u^0 data, especially for the development of comprehensive kinetic mechanisms (e.g., GRI-Mech [2]). Thus, the primary objective of the present program is to devise experimental approaches which would meet such a need. Our initial goal was 60 atm because of its relevance to internal combustion engines, both reciprocating and continuous. The challenge of attaining an order of magnitude increase in the coverage of the pressure range is particularly noteworthy.

Recent determinations of s_u^0 have utilized the counterflow flame and the outwardly propagating flame. Specifically, by using the counterflow flame, s_u^0 values were determined up to 6–7 atm for methane/air mixtures in our laboratory. The limitation appears to be caused by instability due to the increase in the flow Reynolds number with increasing pressure. Although this effect can be somewhat mitigated by using nozzles of smaller diameter, the nozzle size must be of a similar magnitude as the nozzle separation distance, which in turn is restricted by the flame thickness and radial dimension, such that the flame can still be considered planar.

An alternate means of measuring s_u^0 is to use the spark-ignited, outwardly propagating flame in an enclosed chamber. The traditional approach [3], based on pressure variations in a windowless chamber, allows experimentation with very high initial pressures. However, without direct observation of the flame movement and hence the ability to evaluate the stretch intensity, it is fundamentally not acceptable for our purpose. Furthermore, it is also not possible to assess the effects of flame shape distortion due to buoyancy and the development of flame front cellular instabilities. Finally, the continuously changing temperature and pressure of the unburned mixture imposes significant challenge in the accuracy of data reduction.

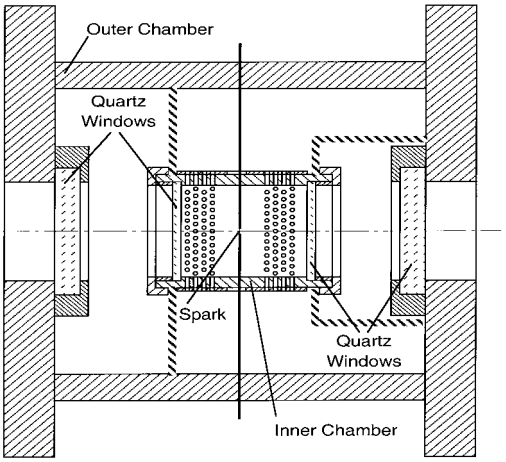

FIG. 1. Schematic of experimental apparatus. Inner vessel: 82.55 mm inside diameter and 127 mm length. Outer chamber: 273.05 mm inside diameter and 304.8 mm length. Quartz windows: 92 mm diameter.

Groff [4] first measured spherical flame speeds at high pressures, up to 5 atm, by directly imaging the propagating flame front and also through pressure measurements. Lately, Taylor and coworkers [5–7] and Faeth and coworkers [8–13] determined s_u^0 values for various fuel compositions and pressures through systematic subtraction of stretch effects using similar imaging techniques. The values s_u^0 so determined, with different stretch-compensated relations, are in reasonably good agreement with each other, as well as with computational calculations and the data from counterflow experiments. These experiments, however, have been limited to pressures lower than 3–4 atm. Recently, Bradley and coworkers [14] made limited measurements of s_u^0 for near-stoichiometric iso-octane/air mixtures up to 10 atm. The limiting complication is the facilitated onset of flame front instability due to the decreased flame thickness at higher pressures.

For the present work, we adopted the spark-ignited, outwardly propagating flame approach because of the inherent flow limitation and design complication involved with the counterflow flame. We nevertheless developed a novel experimental design which allows direct imaging of the flame, for near-constant-pressure propagation, up to 60 atm. Consequently, flame images amenable for qualitative understanding and quantitative analysis of various aspects of the flame morphology and propagation were obtained for such a high-pressure range. In and by itself, we believe the experimental design is a useful contribution to the study of high-pressure combustion phenomena. Furthermore, we explored means to delay the onset of flame front instability such that the pressure range over which s_u^0 can be determined from smooth flames is substantially extended from previous studies. Hydrogen was used in the present investigation because its chemistry is relatively simple and well studied. Furthermore, since it is highly susceptible to the diffusional-thermal cellular instability, it provides a worst-case study on the interference of flame front instability [15] in the determination of s_u^0.

Experiment

Apparatus

Figure 1 shows the schematic of the apparatus. The apparatus consists of two concentric, cylindrical vessels: an inner vessel initially filled with the combustible mixture and an outer chamber initially filled with an inert, at the same pressure. For optical access, quartz discs comprise the circular ends of the inner vessel, and quartz windows are mounted in the end caps of the outer chamber. The lateral walls of the inner vessel and an encasing cylindrical sleeve contain matching rows of holes which, when offset, seal via O-rings the inner vessel from the surrounding outer chamber. Just prior to ignition, the encasing sleeve of the inner vessel is mechanically translated, in a pistonlike manner, such that the rows of holes align, establishing continuity between the two vessels. Flame propagation terminates as it reaches the wall of the inner vessel, thereby preventing excessive pressure buildup within the chamber. Furthermore, since the volume of the inner vessel is 25 times smaller than that of the outer chamber, the total pressure increase due to combustion is small, ensuring operational safety and allowing optical investigation. The apparatus has been tested to a maximum operating pressure of 95 atm.

The reactant mixtures were prepared within the inner vessel using partial pressures. All runs were performed in quiescent environments at an initial temperature of 298 K and initial pressures ranging from 1 to 60 atm.

Flame propagation was initiated via spark discharge, with an adjustable gap to within 10 μm, at the center of the inner vessel. Spark durations ranged from 5 to 10 μs, and the energies were adjusted to be close to the minimum ignition energies (5–20 mJ) to minimize effects of initial flame acceleration by excessive spark energies.

Instrumentation

Measurements involved observing the flame propagation using Schlieren cinematography. The system is based on a 100 W mercury short-arc lamp, with the light collimated and condensed by lenses, and the flame images were captured using a high-speed digital-video camera operating at 2000–8000 fps. An

absolute-pressure transducer monitored the inner vessel, and a differential-pressure transducer monitored the pressure between the two chambers, with the histories recorded by a digital oscilloscope.

Data Reduction

Since the burned gas is motionless for the outwardly propagating spherical flame, the experimentally visualized flame front motion is the burned flame speed. Experimental data were analyzed using the data-fitting technique of Taylor and coworkers [5–7], based on the linear extraction of unstretched burned flame speed, s_b^0, and Markstein length, L_b. Specifically, $s_b = \dot{R} = s_b^0/(1 + 2L_b/R)$, which on integration yields an equation that correlates the experimentally measured flame radius with time—namely, $R + 2L_b \ln(R) = s_b^0 t +$ constant—from which s_b^0 and L_b can be obtained via linear regression. With s_b^0 known, s_u^0 is obtained by dividing s_b^0 by the computed density ratio of the corresponding planar flame. The standard error in measuring the flame position is ~3%.

Numerical Simulations

The planar, adiabatic, one-dimensional premixed flame was simulated using the flame code developed by Kee et al. [16]. A reaction mechanism involving 9 species and 21 elementary reactions was taken from Mueller et al. [17]. Third-body efficiency factors for argon were used for helium, and Soret effects were included. Adaptive gridding was used to resolve the details of the flame structure. The discretization was reduced until no change was observed in the solution to ensure convergence. Inclusion of radiative heat loss was found to have minimal influence (<1% difference between adiabatic and optically thin) for the experimental conditions examined, even up to the limit of 20 atm calculated herein.

For all calculations, the unburned-mixture temperature was 298 K, the burned boundary had zero gradients, and the computational domain was chosen to be sufficiently large (25 m).

Results and Discussion

Flame Morphology

As was well established in previous studies, cellular instabilities develop over the flame surface at various stages in its propagation and can severely limit the system parametric range over which wrinkle-free flame speeds can be determined. Specifically, thermal-diffusive instability is promoted for Markstein lengths smaller than certain critical values. For example, Kwon et al. [8] found that for 3 atm hydrogen/air flames, only flames with equivalence ratio, ϕ, greater than ~1.4 (or positive Markstein length) are not severely affected by thermal-diffusive instability. Sun et al. [18] also computationally found that for hydrogen/air flames the Markstein length becomes positive at $\phi = 0.7$, 0.9, and 1.3 for pressures of 0.6, 1, and 5 atm, respectively. Thus, we expect that as pressure increases, the thermal-diffusive instability occurs over an increasing range of ϕ, spanning from the entire lean regime to part of the moderately rich regime. Furthermore, thermal-diffusive cells are small—of the dimension of the flame thickness—and their onset is moderated by the positive stretch of the outwardly propagating flame [19].

The flame is also susceptible to hydrodynamic instability of all wavelengths. They are expected to appear initially in large dimensions, being triggered by system-based perturbations, and cascade down to smaller cells until they reach a size similar to that of the thermal-diffusive cells when they are stabilized by the curvature.

Two strategies were implemented to delay the onset of flame front instability so that the period of flame propagation with a smooth flame surface could be extended to allow for sufficient data for extrapolation to the state of stretch-free flame. The first is to conduct experiments using inert-diluted mixtures. This weakens the flame, increases its thickness, reduces the density gradient and hence the baroclinic torque across it, and consequently weakens the development of the hydrodynamic instability. The second is to use helium as the diluent. This increases the Lewis number of the flame, hence retarding the formation of thermal-diffusive cells. The helium-diluted flame is also thicker, which further retards the formation of cells.

Having recognized the above features and provisions, we now present our results on the morphology of the flame as it propagated outward in various environments (Fig. 2). First, for propagation at 1 atm pressure and 21% O_2 with either nitrogen or helium as the diluent, the flame surface remained smooth throughout the observation period, similar to some of the smooth images shown in Fig. 2. Fig. 2a shows propagation in 3 atm, 12.5% O_2, for $\phi = 0.70$ and 2.25, and with either nitrogen or helium as the diluent. It is seen that, for the nitrogen-diluted mixtures, the flame remained smooth for the rich flame while instabilities developed for the lean flame. Furthermore, the large hydrodynamic cells were first developed, at about 4.0 ms, and were followed by the development of the small thermal-diffusive cells which were uniformly distributed over the flame surface and imparted to it a rugged contour. For the helium-diluted lean flame, it is significant to note that development of all cells was suppressed, although the upper electrode seems to have

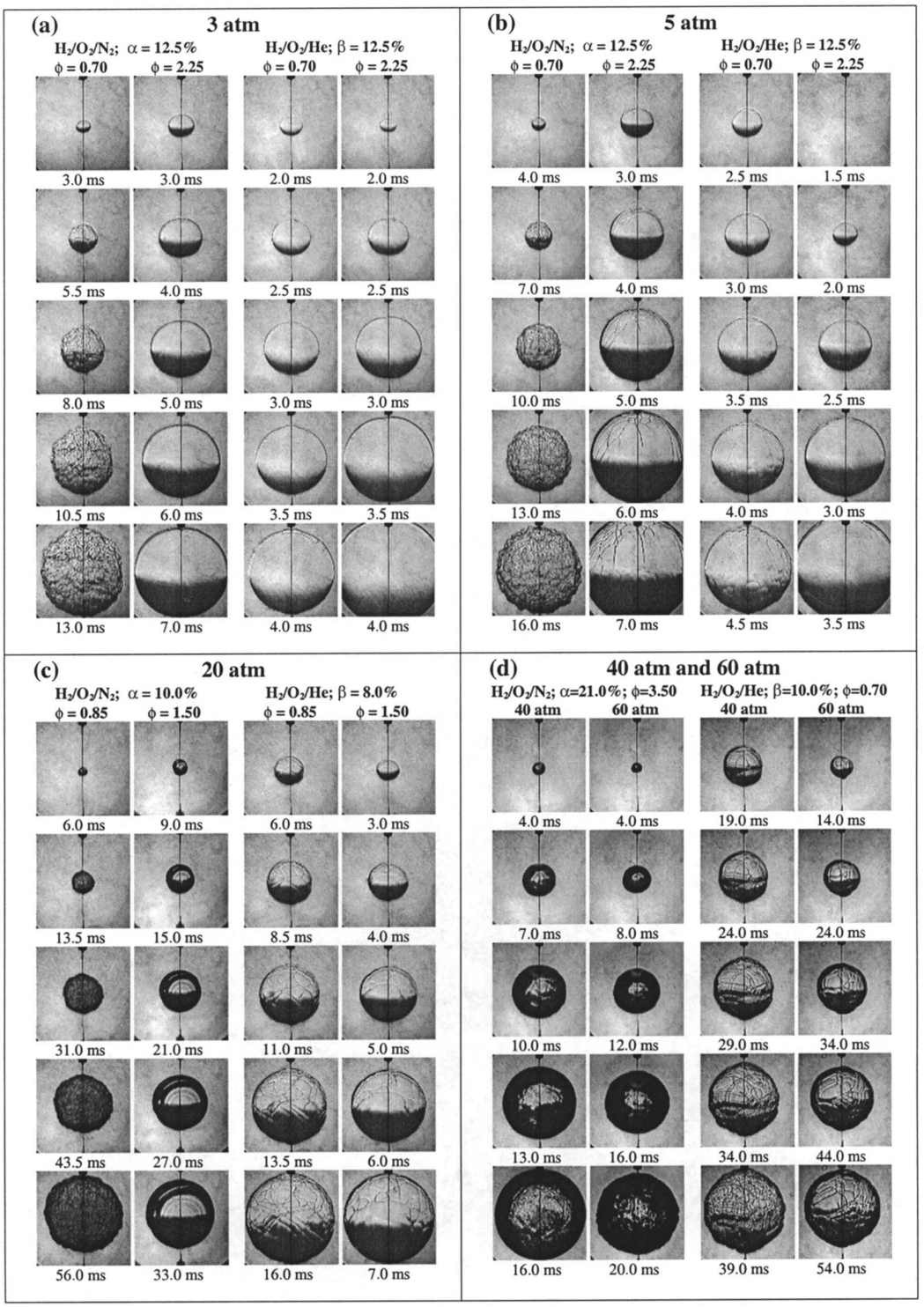

FIG. 2. Schlieren photographs (horizontal knife edge) of $H_2/O_2/N_2$ and $H_2/O_2/He$ flames under lean and rich conditions at (a) 3 atm, (b) 5 atm, (c) 20 atm, and (d) 40 and 60 atm. $\alpha = O_2/(O_2 + N_2)$. $\beta = O_2/(O_2 + He)$. N_2-diluted flames below $\alpha = 10\%$ could not be ignited. Scale: frame diagonal is 74 mm.

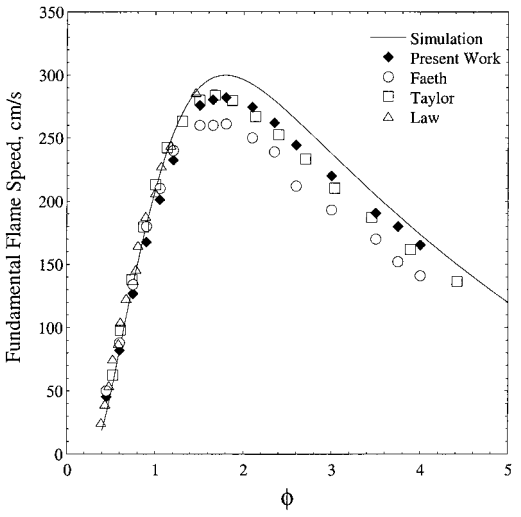

FIG. 3. Measured and calculated unstretched laminar flame speeds as a function of fuel equivalence ratio for hydrogen/air flames at standard temperature and pressure. Measurements are from Taylor [6], Faeth and coworkers [11], Law and coworkers [20–22], and the present study. Calculations are based on the kinetics of Mueller et al. [17]. Symbols represent experimental data; line represents calculation.

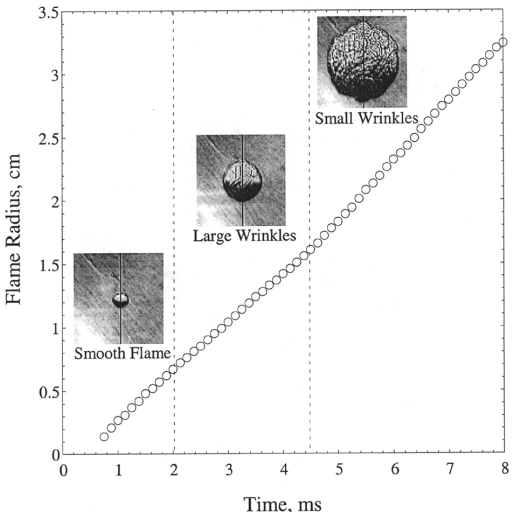

FIG. 4. Flame radii versus time for $H_2/O_2/N_2$ flame with $O_2/(O_2 + N_2) = 0.125$ at unity equivalence ratio and 3 atm.

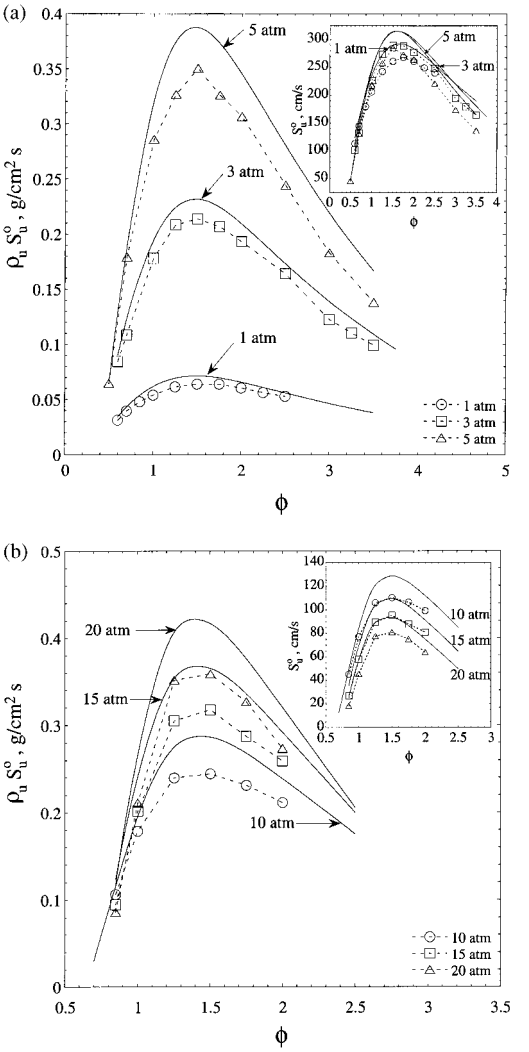

FIG. 5. Measured and calculated unstretched laminar mass burning rates as a function of fuel equivalence ratio for H_2/O_2/He flames at (a) 1, 3, and 5 atm, where $O_2/(O_2 + He) = 0.125$, and (b) 10, 15, and 20 atm, where $O_2/(O_2 + He) = 0.08$. Calculations are based on the kinetics of Mueller et al. [17]. The inset shows the corresponding unstretched laminar flame speeds. Symbols represent experimental data; lines represent calculation.

induced some wrinkles. The helium-diluted rich flame, of course, remained smooth throughout.

Development of cells was further promoted when the pressure was increased to 5 atm, as shown in Fig. 2b. The cell development for the nitrogen-diluted lean flame remained similar to that of the 3 atm flame, except it was initiated earlier. However, instabilities that were clearly hydrodynamic in origin then developed for the rich flame, through the appearance of large-scale "cracks" or "wrinkles." For the

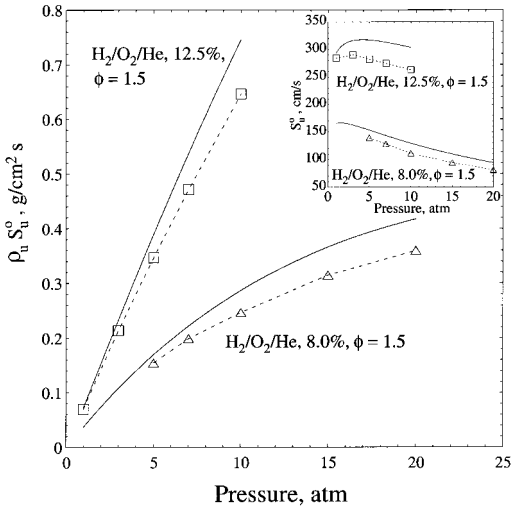

FIG. 6. Measured and calculated unstretched laminar mass burning rates for $H_2/O_2/He$ flames at fixed equivalence ratios as a function of initial pressure. Calculations are based on the kinetics of Mueller et al. [17]. The inset shows the corresponding unstretched laminar flame speeds. Symbols represent experimental data; lines represent calculation.

helium-diluted flames, cells developed for the lean flames. These cells were fairly large and were hydrodynamic in nature. The rich helium-diluted flame remained relatively smooth.

With further increase of pressure to 20 atm (Fig. 2c), cell formation was greatly facilitated. In an effort to retard their formation, the oxygen concentration was further reduced. Thermal-diffusive cells were formed for the lean nitrogen-diluted flames, and hydrodynamic instabilities overwhelmed the rich nitrogen-diluted flames. For helium-diluted flames, the thermal-diffusive cells were suppressed, although the hydrodynamic cells formed readily, covering the flame surface with cells of moderate sizes.

Finally, Fig. 2d shows the flame morphology at 40 and 60 atm for nitrogen-diluted flames at rich conditions and helium-diluted flames at lean conditions. Considering the mixture composition of these flames, the surface irregularities are hydrodynamic in nature. The images also show that initiation of the cell is much more advanced for the nitrogen-diluted flames.

Determination of Laminar Flame Speeds

As a benchmark for the reliability and accuracy of the new experimental results, Fig. 3 plots s_u^0 as a function of ϕ for hydrogen/air mixtures at standard temperature and pressure, along with the stretch-corrected results from Taylor and coworkers [5,6], Faeth and coworkers [11], Law and coworkers [20–22], and the numerical simulation with the aforementioned kinetic mechanism. Results from all sources agree well with each other for the lean flames. For the rich flames, the present results agree well with those of Taylor and coworkers [5,6] but are higher than those of Faeth and coworkers [11]. All experimental data, however, are consistently smaller than the calculated ones on the rich side, indicating the possible weakness in the kinetic mechanism, which becomes observable for rich mixtures.

Figure 4 shows a typical plot of the flame radius versus time for a flame exhibiting the transitions from a smooth surface, to one with few to moderate amounts of the large, hydrodynamic wrinkles, to one densely populated with small wrinkles, which could be either hydrodynamic or thermal diffusive in nature. While the quantification of "large" and "small" wrinkles is not precise, the general trend is that large wrinkles seem to affect the flame speed minimally or at most moderately, while small wrinkles increase the propagation speed substantially. For the extracted flame speed, s_u^0, reported in the following, all data for 1, 3, and 5 atm were obtained from flames that were wrinkle free. For the 10, 15, and 20 atm data, there were just one or two wrinkles toward the later part of the period over which the data were analyzed. A two-dimensional cut of the flame surface was smooth, with "cracks" of small magnitude appearing only within the visualized flame interior. Data analysis typically started from when the ignition transient was over, and the flame had assumed a smooth, spherical shape. Only flame-radii data less than 25 mm were analyzed. Beyond 20 atm, all flames were unstable practically from inception, and flame speed measurements could not be made.

Figure 5 shows the stretch-corrected mass burning rates, $\rho_u s_u^0$ (as well as s_u^0 in the inset), and the corresponding calculated values for hydrogen-diluted flames at 1, 3, 5, 10, 15, and 20 atm. The data for 1, 3, and 5 atm (Fig. 5a) were obtained with $O_2/(O_2 + He) = 12.5\%$ dilution, while those for 10, 15, and 20 atm (Fig. 5b) were obtained with 8% dilution. More dilution is necessary at the higher pressures to suppress instabilities. Fig. 5a shows overall favorable agreement between the experiments and the simulations, with the experiments consistently lower than the simulations, as also displayed for the 1 atm H_2/air case (Fig. 3). At higher pressures, the comparison is still quite acceptable, however, with the experimental data even lower than the simulations.

Figure 6 shows the effect of pressure on the stretch-free mass burning rates, $\rho_u s_u^0$, for some selected mixtures. The comparisons are good, especially considering that there exists very little validation for the kinetic mechanism under rich conditions. Moreover, for rich mixtures, the uncertainties in molecular transport for the H atom may also affect the predictions.

Finally, it is worth noting that the efficiency factors used for monatomic He were those of Ar, as specified in the mechanism [17] for termolecular reactions. Since third-body termination reactions such as $H + O_2 + M \rightarrow HO_2 + M$ become significant at elevated pressures, the uncertainty in these values can create considerable differences in the predicted flame speeds. Further investigation of these parameters is needed.

Concluding Remarks

Previously unexplored morphology of constant-pressure, expanding spherical flames at elevated pressures up to 60 atm was examined. Results show that flame instabilities dominated flame dynamics at these elevated pressures, especially the development of hydrodynamic cells, which would occur for all fuels and equivalence ratios. This is clearly a factor that needs to be seriously considered in studying processes within internal combustion engines.

We also demonstrated that helium dilution is a viable technique to suppress instabilities for laminar flame measurements, with new stretch-free flame-speed data extracted for H_2/O_2/He mixtures from lean to rich conditions up to 20 atm. Recognizing previous limitations on the attainable maximum pressure, the availability of the present data for the study of kinetic mechanisms is emphasized. Moreover, the present results indicate the need for examining the uncertainties in third-body efficiency factors and transport coefficients, especially for high pressures and extensive equivalence ratio ranges. Finally, the uniqueness and capability of the present apparatus, which required considerable effort in development, offer potential for the in-depth study of other transient, high-pressure flame initiation and propagation phenomena.

Acknowledgments

This work was supported by NASA grant NCC3-687. Special thanks are due to Mr. Gilberto Rozenchan for help with the experiments, Mr. Erik Christiansen for help with the numerical simulations, Dr. Kurt Sacksteder for acquiring the diagnostic equipment, and Dr. Mark Mueller for valuable advice and discussions.

REFERENCES

1. Wu, C. K., and Law, C. K., *Proc. Combust. Inst.* 20:1941–1949 (1985).
2. Smith, G. P., Golden, D. M., Frenklach, M., Moriarty, N. W., Eiteneer, B., Goldenberg, M., Bowman, C. T., Hanson, R., Song, S., Gardiner, W. C., Lissianski, V., and Qin, Z., http://www.me.berkeley.edu/gri_mech/, U.C. Berkeley, Berkeley, CA (1999).
3. Metghalchi, M., and Keck, J. C., *Combust. Flame* 38:143–154 (1980).
4. Groff, E. G., *Combust. Flame* 48:51–62 (1982).
5. Dowdy, D. R., Smith, D. B., Taylor, S. C., and Williams, A., *Proc. Combust. Inst.* 23:325–332 (1990).
6. Taylor, S. C., "Burning Velocity and the Influence of Flame Stretch," Ph.D. thesis, University of Leeds, 1991.
7. Brown, M. J., McLean, I. C., Smith, D. B., and Taylor, S. C., *Proc. Combust. Inst.* 26:875–881 (1996).
8. Kwon, S., Tseng, L.-K., and Faeth, G. M., *Combust. Flame* 90:230–246 (1992).
9. Tseng, L.-K., Ismail, M. A., and Faeth, G. M., *Combust. Flame* 95:410–426 (1993).
10. Hassan, M. I., Aung, K. T., and Faeth, G. M., *J. Prop. Power* 13:239–245 (1997).
11. Aung, K. T., Hassan, M. I., and Faeth, G. M., *Combust. Flame* 109:1–24 (1997).
12. Aung, K. T., Hassan, M. I., and Faeth, G. M., *Combust. Flame* 112:1–15 (1998).
13. Hassan, M. I., Aung, K. T., and Faeth, G. M., *Combust. Flame* 115:539–550 (1998).
14. Bradley, D., Hicks, R. A., Lawes, M., Sheppard, C. G. W., and Wooley, R., *Combust. Flame* 115:126–144 (1998).
15. Bradley, D., and Harper, C. M., *Combust. Flame* 99:562–572 (1994).
16. Kee, R. J., Grcar, J. F., Smooke, M. D., and Miller, J. A., Sandia report SAND85-8240.
17. Mueller, M. A., Kim, T. J., Yetter, R. A., and Dryer, F. L., *Int. J. Chem. Kinet.* 31:113–125 (1999).
18. Sun, C. J., Sung, C. J., He, L., and Law, C. K., *Combust. Flame* 118:108–128 (1999).
19. Bechtold, J. K., and Matalon, M., *Combust. Flame* 67:77–90 (1987).
20. Egolfopoulos, F. N., and Law, C. K., *Proc. Combust. Inst.* 23:333 (1990).
21. Law, C. K., in *Reduced Kinetic Mechanisms for Applications in Combustion Systems* (N. Peters and B. Rogg, eds.), Springer-Verlag, Berlin, 1993, p. 15.
22. Vagelopoulos, C. M., Egolfopoulos, F. N., and Law, C. K., *Proc. Combust. Inst.* 25:1341 (1994).

COMMENTS

Jerry Lee, ETH Zurich, Switzerland. The flame is always positively stretched, and one has to rely upon extrapolation to the limit of the large radius of the "flame ball," but on the other hand as R increases, the flame becomes unstable, and thus the data become less reliable. How do you mitigate this? In fact, as R increases the effect of buoyancy increases as well, which further degrades the data.

Author's Reply. As described in detail in the paper, we diluted the H_2/O_2 mixtures with helium in order to suppress instabilities (both diffusional-thermal and hydrodynamic) so that new, high-pressure, stretch-free flame speed data could be extracted from smooth, spherical flames. Concerning the effect of buoyancy, it can undoubtedly play a significant role, especially since buoyant forces increase with increasing pressure, as well as with flame size. However, if the characteristic time for flame propagation is much smaller than that for buoyant convection, then the effect of gravity should be small, as is the case for the hydrogen mixtures in the equivalence ratio ranges, flame radii, and pressures examined. Again, note that we extract fundamental flame speeds at stretch rates and flame radii where the flames are smooth, spherical, and concentric with respect to our ignition source. Nonetheless, for any examination of near-limit phenomena where gravity effects become pronounced, testing in microgravity facilities would be requisite.

•

David Smith, University of Leeds, UK. The paper reports an elegant extension to the expanding flame technique, taking it to higher pressures than hitherto possible. One expects without reserve the need to minimize flame wrinkling and cracking, if the aim is to measure stretch-free burning velocities. But the use of the diluent to achieve this has the drawback that the data are not immediately relevant to practical situations. The obvious route (as taken here) is to use the data to validate kinetic models, but as is well accepted, burning velocities of most fuels are sensitive to relatively few reactions, making this of only partial use. (I suspect in this work the key sensitive reaction will be $H + O_2 + M$, where the relative third-body efficiency of He and N_2 are not well established.)

A second consequence of He dilution is that any Markstein lengths derived are also for an "artificial" mixture. A further consequence of pushing the technique to these high pressures is that, even with He dilution, wrinkling occurs as the flames grow. This, of course, means that only small radii data are available for extrapolation to the stretch-free limit. The extrapolation method must then be reliable, and it is arguable that none of the existing methods are sufficiently reliable.

Author's Reply. With respect to helium dilution, the authors agree that the mixtures are presently not of practical use; and consequently, Markstein lengths were not reported in our work. Nonetheless, fundamental flame speed data is still considered necessary at elevated pressures spanning extensive equivalence ratio ranges for comprehensive chemical kinetic validation. Furthermore, with the aforementioned uncertainties in third-body efficiencies, as well as with molecular transport properties (e.g., H atom, He), the new data become even more valuable. Concerning the extrapolation of fundamental flame speed at small radii and high stretch rates due to inherent flame instabilities, it is exactly due to the commented reasoning that we presented such data for only up to 20 atm. However, our technique goes much farther beyond the measurement of laminar flame speeds; it offers the means for in-depth study of other exciting phenomena, such as ignition, flame instability, self-turbulization, and even DDT, under high pressures.